International Journal of Pharmaceutics: X 8 (2024) 100292

Contents lists available at ScienceDirect

International Journal of Pharmaceutics: X

journal homepage: www.sciencedirect.com/journal/international-journal-of-pharmaceutics-x

Study on the preparation of stabilizer-free silymarin nanocrystals and its oral absorption mechanisms

Liangxing Tu [a], Ping Han [a], Yongbing Sun [a], Yi Jin [a], Kaili Hu [c], Meng Cheng [a,*], Yisen Shao [a,*], Jianfang Feng [a,b,*], Fangying Yuan [a,*]

[a] Jiangxi University of Chinese Medicine, Nanchang 330006, PR China
[b] Guangxi University of Chinese Medicine, Nanning 530200, PR China
[c] Shanghai University of Traditional Chinese Medicine, Shanghai 201203, PR China

ARTICLE INFO

Keywords:
Nanocrystals
Silymarin
High-pressure homogenization method
Physicochemical properties
Absorption mechanism
Pharmacokinetics

ABSTRACT

Many researchers have studied the oral absorption mechanisms yet, however, considering stabilizers often participate in the absorption process of nanocrystals, these known mechanisms may be incorrect. Hence in this study, we aimed to explore the correct absorption mechanism of nanocrystals by performing related studies on stabilizer-free nanocrystals. We firstly prepared stabilizer-free silymarin nanocrystals by high-pressure homogenization, and then performed absorption-related studies, such as solubility, dissolution rate, pharmacokinetic study, cellular uptake and intracellular transport. Results showed the stabilizer-free silymarin nanocrystals had an average particle size of (450.2 ± 4.46) nm, with PDI of 0.280 ± 0.021 and Zeta potential of −26.9 ± 2.4 mV. The conversion of silymarin crude drug to stabilizer-free silymarin nanocrystals increased the compound's solubility by 1.41 times, with a dissolution rate of 92.2 % in water within 30 min compared to 38.5 % for crude drugs. Pharmacokinetic studies showed the oral bioavailability of stabilizer-free silymarin nanocrystals was found to be 1.48 times greater than that of the crude drugs. The cell experimentation results demonstrated that the stabilizer-silymarin nanocrystals can improve uptake but have poor transmembrane transport properties. Most researchers believe that nanocrystals can enhance transmembrane transport of drugs via an endocytosis-mediated pathway. In fact, nanocrystals are indeed endocytosed more by the cells, but this transport pathway is poor because the cells lack the intracellular transport pathway to transport nanocrystals from the AP side to the BP side. Therefore, we believe that the intracellular transport of nanocrystals can be enhanced by modifications and other carriers if needed to improve nanocrystals' ability to promote oral absorption.

1. Introduction

Oral administration is currently the most popular route of drug delivery due to its cost-effectiveness and high patient compliance. However, a significant challenge arises as more than 90 % of new chemical entities and approximately 65–70 % of drug molecules have poor solubility in water, leading to limited oral bioavailability (Goke et al., 2018; Yi et al., 2015; Lu et al., 2016; Tu et al., 2020a). Researchers have discovered that utilizing drug nanocrystals can enhance the bioavailability of poorly soluble drugs through mechanisms such as biological adhesion, inhibition of P-gp efflux, facilitation of endocytosis-mediated transmembrane transport pathway and suppression of hepatic drug enzyme metabolism (Viswanadh et al., 2020; Kadam et al., 2020; Kirtane et al., 2013; Palle and Neerati, 2017; Wang et al., 2014). Furthermore drug nanocrystals can elevate the saturation solubility and dissolution rate of the drug by reducing the drug nanocrystals particle size (Tu et al., 2020b; Kesisoglou et al., 2007). Therefore, drug nanocrystals are considered a promising technology in the pharmaceutical field to enhance the oral bioavailability of poorly soluble drugs.

The potential of drug nanocrystals to enhance bioavailability is constrained by the need for surfactants or functional polymers as stabilizers. These stabilizers play a crucial role in influencing the oral absorption and in vivo circulation of drug nanocrystals. For instance, sodium dodecyl sulfate (SDS) can loosen tight junction.

and boost drug absorption (Liu et al., 2021; Zhang et al., 2019; Popov et al., 2016). Substances like chitosan, polyvinylpyrrolidone (PVP), polyvinyl alcohol (PVA) possess biological adhesion properties that prolong the interaction between the drug and the gastrointestinal tract,

* Corresponding authors.
E-mail addresses: cmjxzyy@126.com, chengmeng1@jxutcm.edu.cn (M. Cheng), 951055049@qq.com, yuanfangying1@jxutcm.edu.cn (F. Yuan).

https://doi.org/10.1016/j.ijpx.2024.100292
Received 5 July 2024; Received in revised form 30 September 2024; Accepted 9 October 2024
Available online 10 October 2024

thereby enhancing oral absorption (Liu et al., 2019; Ponchel et al., 1997; Maisel et al., 2015). Stabilizers with P-glycoprotein (P-gp) inhibition can facilitate drug absorption by inhibiting drug efflux or increasing drug intestinal retention. Exploring the oral absorption mechanism of stabilizer-free drug nanocrystals could serve as a valuable foundation for further advancements in enhancing the oral absorption of poorly soluble drugs through nanocrystal technology, leading to the development of oral formulations.

Silymarin, a natural flavonoid extracted from *Silybum marianum* and its main conponents are taxifolin (TX), silychristin (ST), silydianin (SDN), silybin A (SB), silybin B (SB), isosilybin A (ISA) and isosilybin B (ISB) (Lu et al., 2007; Kvasnicka et al., 2003; Ding et al., 2001; Zhu et al., 2013), has shown significant hepatoprotective effects in various experimental liver injuries (Lee et al., 2005; Choi et al., 2005; Wei et al., 2015a). Its ability to scavenge free radicals has led to its clinical use in treating specific liver complications (Burczynski et al., 2012; Bahmani et al., 2015). Notably, silymarin is well-tolerated by both animals and humans, even at high doses. However, the poor solubility and low surface area of silymarin particles can lead to reduced bioactivity at higher drug doses (Shangguan et al., 2014; El-Nahas et al., 2017; Hwang et al., 2014). Currently, efforts to enhance the water solubility of silymarin include complexing it with phosphatidylcholine (Federico et al., 2015; Xu et al., 2013) and lecithin (Morazzoni et al., 1992; Raj et al., 2010; Abrol et al., 2005), as well as utilizing techniques; such as cyclodextrin inclusion complexes (Arcari et al., 1992; Ghosh et al., 2011) and solid dispersions (Li and Hu, 2004). While a commercial product (Legalon® is a phospholipid complex formulation of silymarin) containing silymarin is available, there have been no reported attempts to prepare stabilizer-free silymarin nanocrystals using high-pressure homogenization and evaluate them in vitro and in vivo (Yang et al., 2013). This study aimed to use silymarin as a model drug to prepare stabilizer-free silymarin nanocrystals, which were then assessed for their oral absorption mechanism both in vitro and *vivo*.

2. Materials and methods

2.1. Materials

Silymarin, silymarin crude drugs, and hesperidin were purchased from Xinyang Mufan Biological Technology Co., Ltd. Povidone K30 (PVP K30) was obtained from Boaixin Open Source Medical Technology Co., Ltd. Sodium dodecyl sulfate (SDS), potassium dihydrogen phosphate, sodium hydroxide, hydrochloric acid, and formic acid (analytically pure) were purchased from Xilong Technology Co., Ltd. Poloxamer P188 was acquired from Beijing Solarbio Technology Co., Ltd. Ltd.; Tween 80 was purchased from Tianjin Damao Chemical Reagent Factory; methanol and acetonitrile (analytically pure) were purchased from Fisher, USA; glacial acetic acid was purchased from Guangdong Guanghua Technology Co., Ltd.; sodium acetate was purchased from Shanghai Lingfeng Chemical Reagent Co. Ltd.; DMEM high glucose medium, non-essential amino acids, 0.25 % EDTA trypsin, and PBS buffer were procured from Beijing Solarbio Technology Co., Ltd. The BCA protein kit was obtained from Dalian Meilun Biotechnology Co., Ltd. Verapamil (D1925074, 99 %) and chlorpromazine (H1926054, 98 %) were purchased from Aladdin. Colchicine (C12696771, 98 %) and indomethacin (C11861101, 99 %) were procured from Macklin. Quercetin (100081–201,610, 99.8 %) was procured from the China Institute for Food and Drug Control. Sodium aside was obtained from other research groups in the laboratory. Fetal bovine serum was purchased from Gibco, USA. The transwell plate, 24-well plate and 96-well plate were purchased from Costar, USA. Acetonitrile (chromatographically pure) was bought from Fisher, USA, while anhydrous ethanol (analytical purity) was procured from Chemical Reagents Co. Ltd. Male SD rats (200-250 g) were purchased from Changsha SLAC Laboratory Animal Co. Ltd.

2.2. Preparation and characterization of stabilizer-free silymarin nanocrystals

In the study, silymarin crude drug was accurately weighed and dissolved in 50 mL of pure water. The initial suspension was generated through high shear dispersion is 16,000 r/min, then transferred to a high-pressure homogenizer and homogenized multiple times under a designated homogenization pressure. Optimal operating conditions were determined through single-factor testing. The investigation assessed the influence of varying drug concentration (0.02 %, 0.1 %, 0.2 %, and 0.3 %), high shear dispersion times (5 min, 10 min, and 15 min), high- pressure homogenization pressures (600 bar, 800 bar, and 1000 bar), and high-pressure homogenization times (5 cycles, 10 cycles, and 15 cycles) on the process of preparing stabilizer-free silymarin nanocrystals. Particle size and polydispersity index (PDI) of the drug nanocrystals were used as criteria to identify the optimal stabilizer-free silymarin nanocrystals formulation. Three sets of samples were simultaneously prepared using the final prescription and process to validate the method. The drug nanocrystals produced were analyzed by using the following techniques:

The Zeta sizer Nano ZS90 instrument (Malvern Instruments Ltd., Malvern, UK) was used to measure the particle size, PDI and Zeta potential of stabilizer-free silymarin nanocrystals. Morphological examination of stabilizer-free silymarin nanocrystals was performed with a transmission electron microscope (TEM, JEM2100, JEOL, Japan). The NCs were diluted with distilled water to a concentration and deposited onto copper mesh. The copper mesh was then negatively stained with 1 % (*w/v*) aqueous solution of phosphotungstic acid. After drying, the copper mesh was observed under TEM. The shape and overall appearance of the stabilizer-free silymarin nanocrystals were examined with scanning electron microscopy (SEM, Quanta 250, FEI, America). The crystal structure of drug nanocrystals was analyzed through differential scanning calorimetry (DSC, Q50, TA, America) and X-ray powder diffraction (XRD, D/Max2500PC, Rigaku Corporation, Japan).

2.3. Study on physicochemical properties of nanocrystals

2.3.1. Drug release study

The dissolution rate of silymarin crude drugs and stabilizer-free silymarin nanocrystals in pure water was investigated using the dialysis bag (MWCO: 8000–14,000) diffusion method. Prepare silymarin crude drugs and stabilizer-free silymarin nanocrystals at a concentration of 5 mg/mL, and take 2 ml into the dialysis bag. Subsequently, the bag was immersed in 200 ml of purified water containing 0.5 % (w/v) SDS at 37 °C. Samples of 2 mL each were collected at time points of 5 min, 10 min, 20 min, 30 min, 40 min, 50 min, 60 min, and 120 min supplemented with distilled water at the same temperature. These samples were then analyzed using HPLC to determine the dissolution rate of each sample.

The HPLC (LC-20 CE, Shimadzu, Japan) conditions were as follows: Diamonsil-C18 column (4.6 mm–250 mm, 5 μm); detection wavelength: 287 nm; mobile phase: methanol-water (45:55); flow rate: 1.0 mL/min; column temperature: 35 °C. Injecting volume: 10 μL.

2.3.2. Solubility study

The saturated solubility of the sample was determined using the shake flask method. Excess silymarin crude drugs and stabilizer-free silymarin nanocrystals were placed in a 5 mL centrifuge tube, followed by the addition of 3 mL of pure water. The sample was then subjected to continuous oscillation at 150 r/min in a constant temperature oscillation chamber at 37 ± 0.5 °C for 24 h. Upon reaching equilibrium, filtration was performed using a 0.22 μm filter, and 1 mL of the filtrate was diluted with methanol for HPLC analysis. The saturated solubility was subsequently calculated based on the standard curve.

2.3.3. Stability study

Stabilizer-free silymarin nanocrystals were prepared and their short-term stability was assessed by measuring changes in particle size and PDI over a 4-day period at room temperature. Drug nanocrystals with common stabilizers such as PVP K30, Tween 80, P188, and SDS (drug: stabilizer =1:2) were also produced using the same method. The study compared the changes in particle size and PDI of stabilizer-free silymarin nanocrystals with those stabilized by traditional stabilizers over the 4-day period, in order to evaluate and compare the stability of drug nanocrystals with and without stabilizers.

2.4. Study on absorption-promoting mechanism

2.4.1. Cellular uptake

MDCK cell suspension at a concentration of 4×10^5 cells/mL was utilized for the experiments. The cells were then seeded into 24-well plates at 0.5 mL per well and incubated for 24 h before removing the culture medium. Subsequently, 0.5 mL of undissolved SM-NC (Stabilizer-free silymarin nanocrystals), undissolved Crude-SM (silymarin crude drug), and dissolved Crude-SM (dissolved in DMSO) were added separately. After 2 h incubation, the drug-containing culture medium was washed away three times with pre-cooled PBS buffer. Following this, 100 μL of trypsin was added to each well for cell digestion, and 200 μL of acetonitrile was introduced. The resulting liquid was then transferred to a 0.5 mL centrifuge tube, vortexed for 3 min, and centrifuged at 12000 r/min for 10 min to collect the supernatant for silymarin content determination. To investigate the absorption pathway of stabilizer-free silymarin nanocrystals, various inhibitors were used in the experiments including Verapamil (100 μM), chlorpromazine (50 μM), indomethacin (100 μM), colchicine (10 μM), quercetin (10 μM) and sodium azide (50 μM). The concentrations of the inhibitors were chosen to be non-toxic to MDCK cells. The stabilizer-free silymarin nanocrystals (250 μM) were incubated with the inhibitors for 2 h to observe drug uptake. Precipitates were stored at 4 °C and analyzed using the BCA protein assay kit ($n = 3$).

A BCA protein quantification procedure was carried out by dissolving 10 mg of protein standard in 1 mL of protein standard preparation solution to create a mother liquid with a concentration of 10 mg/mL. This mother liquid was then diluted with PBS buffer solution to obtain concentrations of 32 μg/mL, 64 μg/mL, 128 μg/mL, 256 μg/mL, 320 μg/mL, 400 μg/mL, and 500 μg/mL. A BCA working solution was prepared by mixing reagent A and reagent B at a 50:1 ratio. To produce 16.32 mL of the solution, 16 mL of BCA reagent A and 0.32 mL of reagent B were combined. The BCA working solution was added to a 96-well plate, followed by the addition of 10 μL of protein standard solution or protein sample to be tested, and then incubated at 37 °C for 30 min. The plate was subsequently analyzed for absorbance at a 562 nm wavelength using a microplate reader. The protein concentration of the sample was determined by referencing the standard curve and considering the dilution factor.

2.4.2. Trans-Membrane transport

MDCK cells were cultured in Transwell chambers with a pore size of 0.4 μm at a density of 2×10^5 cells per well to establish a model. The apical (AP) side received 0.5 mL of cell-containing medium, while the basolateral (BP) side received 1.5 mL of medium. The plates were then placed in an incubator at 37 °C, with daily medium changes over five days. *Trans*-Epithelial electrical resistance (TEER) was recorded, and Trans-epithelial electrical resistance was calculated as (model resistance value - empty membrane resistance value) × monolayer cell model membrane area. A measured TEER $\geq$300 Ω/cm^2 indicated suitability for cell transmembrane transport experiments.

From the AP side to the BL side, an appropriate cell monolayer model was selected. The culture medium in chambers A and B was removed, and 0.5 mL of drug-containing PBS was added to the AP side while 1.5 mL of blank PBS was added.

to the BL side. The chambers were then placed in an incubator at 37 °C. Samples of 0.2 mL were taken from the BL side at 30 min, 60 min, 90 min and 120 min, with an equal amount of blank PBS added each time. For the transfer from the BL side to the AP side, a suitable cell monolayer model was chosen. The culture medium in chambers AP and BL was discarded, and 0.5 mL of blank PBS was added to the AP side while 1.5 mL of drug-containing PBS was added to the BL side. The chambers were placed in the incubator at 37 °C. Samples of 0.2 mL were taken from the AP side at 30 min, 60 min, 90 min and 120 min, with an equal amount of blank PBS added each time. In the hypothermia group, after drug administration, the chambers were placed in a 4 °C refrigerator. 0.5 mL samples were taken from the BL side at 30 min, 60 min, 90 min and 120 min, with an equal amount of blank PBS added after each sampling. To investigate the uptake pathway of the drug nanocrystals, a series of inhibitors (consistent with those inhibiting cellular uptake as previously described) were used for the experiments. All inhibitor concentrations were non-toxic to MDCK cells. The drug was administered in combination with the inhibitors and incubated for 2 h. The transmembrane transport of the drug was then observed ($n = 3$). The apparent permeability coefficient (P_{app}) was calculated as follows:

$$P_{app} = \frac{d_Q}{dt} \bullet \frac{1}{A \bullet C_0} \times 100\%$$

Where d_Q / d_t represents the amount of drug transport per unit time; A is the transport membrane area; C_0 is the initial concentration. Efflux Ratio (ER) = P_{app} (B to A) /P_{app} (A to B), while P_{app} (B to A) is the P_{app} value measured in the B to A direction, and P_{app} (A to B) is the P_{app} value measured in the A to B direction.

2.5. Pharmacokinetic study in vivo

Healthy male SD rats weighing 200–250 g were obtained from Changsha Slake Experimental Animal Co., Ltd. in accordance with Animal Experiment Control and Supervision Committee guidelines. All experiments were approved by the Laboratory Animal Ethics Committee of Jiangxi University of Chinese Medicine (approval number: JZLLSC20240563), and were conducted in accordance with the "Guidelines for the Care and Use of Laboratory Animals". The animals were maintained in a temperature-controlled environment at 25 ± 2 °C with access to feed and water. We randomly divided fifteen rats into three groups, with five rats in each group. The first group received silymarin crude drugs suspension (50 mg/kg) and the second group received the same dose of stabilizer-free silymarin nanocrystals (50 mg/kg). After oral administration, blood samples of 0.3 mL were obtained from the rats' orbital venous plexuses at 0.25 h, 0.5 h, 0.75 h, 1 h, 2 h, 4 h, 6 h, 8 h, 12 h and 24 h. The collected samples were placed in heparinized centrifuge tubes and centrifuged at 4000 r/min for 10 min. Subsequently, the plasma was separated and stored at −20 °C until UHPLC/MS-MS analysis. The third group received a 4 mg/kg dose via tail vein injection, using 20 mg of accurately weighed silymarin that had been dissolved in 5 mL of anhydrous ethanol. Blood samples were collected by retroorbital puncture at various time intervals after administration at 0.0167 h, 0.0833 h, 0.25 h, 0.5 h, 1 h, 2 h, 4 h, 6 h, 8 h, 12 h and 24 h. The blood samples were processed by centrifugation at 4000 r/min for 10 min to separate the plasma, which was then stored at −20 °C until UHPLC/MS-MS analysis.

Plasma sample processing: Measure 50 μL of plasma sample, add 50 μL of internal standard solution, add 50 μL of acetonitrile, vortex and mix for 3 min. Add 50 μL of acetonitrile, vortex and mix for 3 min to fully precipitate the protein, centrifuge at 12000 r/min for 10 min, and take the supernatant into the sample for determination.

The plasma drug concentration was quantitated by UHPLC/MS-MS analysis performed on QRTAP 4500 (AB Sciex, America) with a UHPLC AQ-C18 column (2. Chromatographic column UH1 × 100 mm, 1.8 μm); mobile phase A: 0.1 % formic acid solution, B: acetonitrile; flow rate 0. 35 mL /min; column temperature 30 °C; injection volume 2 μL;

gradient elution; ionization mode: multiple reaction ion detection (MRM); ionic polarization: negative ion; ionization mode: electrospray ionization (ESI). Capillary Voltage 3.50 kV; Drying Gas Temperature 350 °C; Drying Gas Flow Rate 11 L/min; Sheath Gas Temperature 300 °C; Sheath Gas Flow Rate 11 L/min; Nebulizer Pressure 40 psi (1 psi = 6.895 kPa); Silymarin Monitoring Ion Pair *m/z* 482.4 → 301.0; Hesperidin Monitoring Ion Pair m/z 609.3 → 301.0; Ion Polarity: Negative Ions; Ionization Method: Electrospray Ionization (ESI) m/z 609. 3 → 300. 9.

2.6. Statistical analysis

The concentration of the drug in the plasma was calculated using the internal standard method. The data results were analyzed with DAS 3.3.0 pharmacokinetic software. The relative bioavailability (F) was determined using the following formula: $F = \frac{AUC_T \times D_R}{AUC_R \times D_T} \times 100\%$.

The absolute bioavailability (Fabs) was also calculated using the formula: $F_{abs} = \frac{AUC_T \times D_{iv}}{AUC_{iv} \times D_T} \times 100\%$.

(T denotes the test preparation, R denotes the reference preparation, D denotes the dosage, iv denotes the reference preparation for intravenous injection).

3. Results and discussion

3.1. Screening and verification of the prescription process of stabilizer-free silymarin nanocrystals

Fig. 1 (A) illustrates that the particle size of the drug nanocrystals decreases gradually with increasing high shear dispersion time. Once the shear time reaches 10 min, there is minimal additional impact on the particle size, leading to a fixed shear time of 10 min. In Fig. 1 (B), at drug concentrations of 0.02 %, 0.1 %, and 0.2 %, the particle size of the drug nanocrystals was around 450 nm with a PDI below 0.3. However, at a drug concentration of 0.3 %, there was a slight increase in particle size and the PDI exceeded 0.3. Fig. 1 (C) demonstrates that an increase in homogenization pressure results in a decrease in both particle size and PDI of the drug nanocrystals. Increasing the pressure from 800 bar to 1000 bar did not significantly affect the particle size or PDI, with a preference for a pressure of 800 bar for efficiency and energy conservation. Finally, in Fig. 1 (D), it is observed that the particle size and PDI of the drug nanocrystals decrease as the number of homogenization cycles increases. The particle size and PDI did not show significant reduction when homogenized 15 times compared to 10 times. Therefore, 10 homogenization rounds were chosen to balance work efficiency and energy conservation.

Using the optimal prescription process obtained from a single-factor investigation, three batches of stabilizer-free silymarin nanocrystals were concurrently prepared through high-pressure homogenization technology. The process involved weighing 100 mg of silymarin crude drugs, adding them to 50 mL of distilled water, stirring and suspending the mixture, placing it in a high-shear disperser, and shearing at 16000 r/min for 10 min to obtain the initial suspension. Subsequently, the initial suspension underwent high-pressure homogenization at 800 bar for 10 cycles. Analysis of the results showed that the three batches of stabilizer-free silymarin nanocrystals had a milky white appearance with consistent particle sizes of 449.8 ± 7.56 nm, 458.7 ± 8.72 nm, and 450.0 ± 10.82 nm, respectively. This indicates that the quality of the

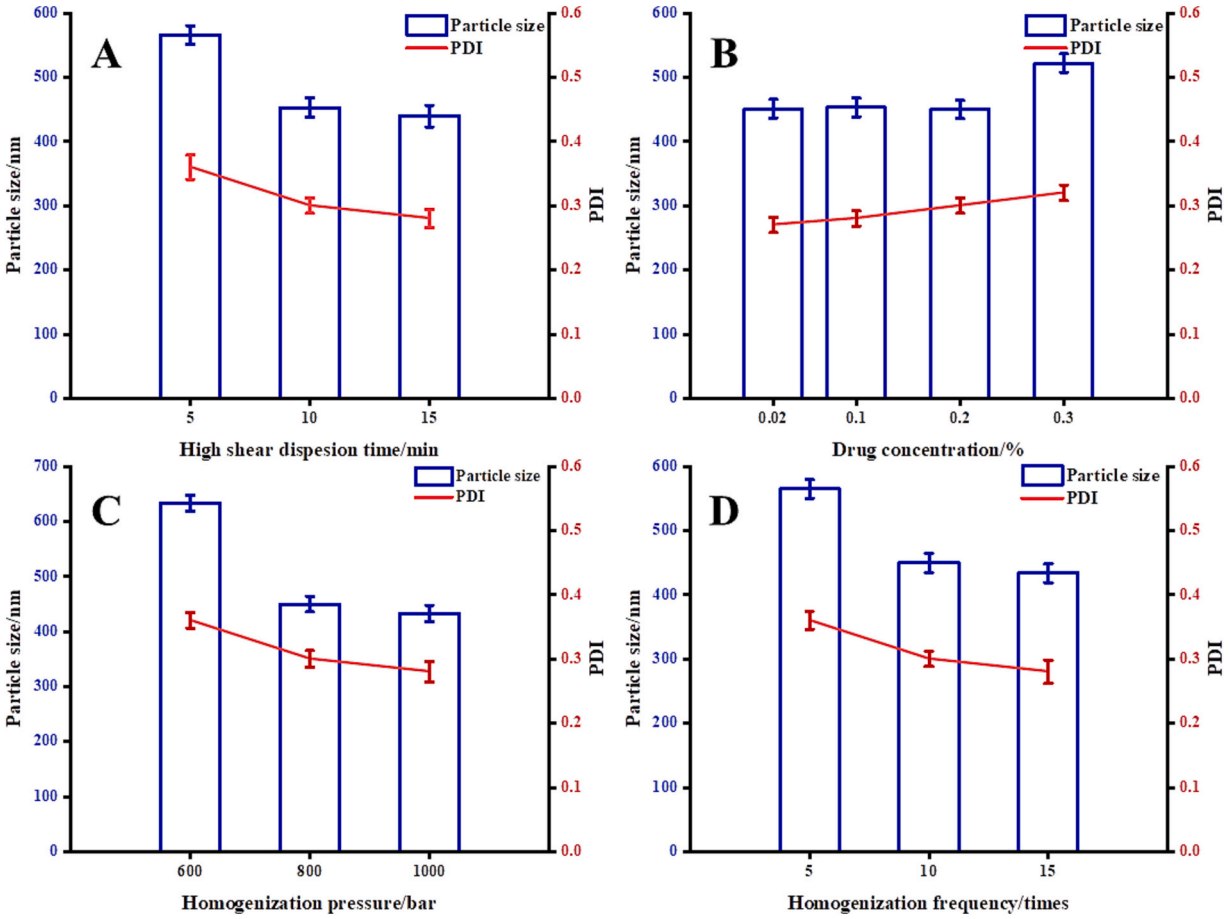

Fig. 1. Effect of high shear dispersion time (A), drug concentration (B), homogeneous pressure (C) and homogeneous frequency (D) on the quality of drug nanocrystals ($n = 3$).

stabilizer-free silymarin nanocrystals in all three batches is comparable, confirming the validated prescription procedure as the optimal one.

3.2. Characterization of stabilizer-free silymarin nanocrystals

The morphology of silymarin crude drugs and stabilizer-free silymarin nanocrystals was observed using scanning electron microscopy and transmission electron microscopy as shown in Fig. 2 (A) (B). The average particle size of stabilizer-free silymarin nanocrystals was (450.2 ± 4.46) nm, the PDI was 0.280 ± 0.021, and the zeta potential was −26.9 ± 2.4 mV, which showed a normal and narrow distribution as shown in Fig. 2 (C). The silymarin crude drug exhibited a particle size range of 2–20 μm with a wide particle size distribution. However, upon conversion to nanocrystals, the particle size was narrowed down to approximately 450 nm, exhibiting uniform particle size distribution with a regular spherical shape. The crystal form of the nanocrystals was analyzed through XRD and DSC. As shown in Fig. 3, the silymarin crude drugs displayed an endothermic peak at 173.52 °C, whereas the stabilizer-free silymarin nanocrystals displayed an endothermic peak at 166.22 °C. The obtained results indicate that the stabilizer-free silymarin nanocrystals persisted in the crystalline form without any alteration in its crystal morphology. However, there was a slight shift in the observed endothermic peak, which could be attributed to the alteration in the crystallinity of the silymarin. Silymarin crude drug exhibited significant diffraction peaks at 15.99°, 17.04°, 20.92°, 22.35°, and 25.38°. Corresponding peaks were also visible for stabilizer-free silymarin nanocrystals, indicating the retention of similar crystal morphology and absence of new crystal forms. The application of high shear and high-pressure homogenization processes did not alter the silymarin crystal form. It is evident from the diagram that the diffraction peak for the drug nanocrystals is less intense than that of the API. This implies that the drug's crystallinity is decreased, aligning with the DSC results.

3.3. Study on physical and chemical properties

3.3.1. Study on the drug release

The results of dissolution behavior of silymarin crude drugs and drugs nanocrystals are shown in Fig. 4 (A). In a pure water medium, the dissolution rate of stabilizer-free silymarin nanocrystals reached approximately 92.2 % within 30 min, whereas the dissolution rate of API was only 38.5 %. The utilization of nanocrystal technology notably enhanced the dissolution rate of silymarin.

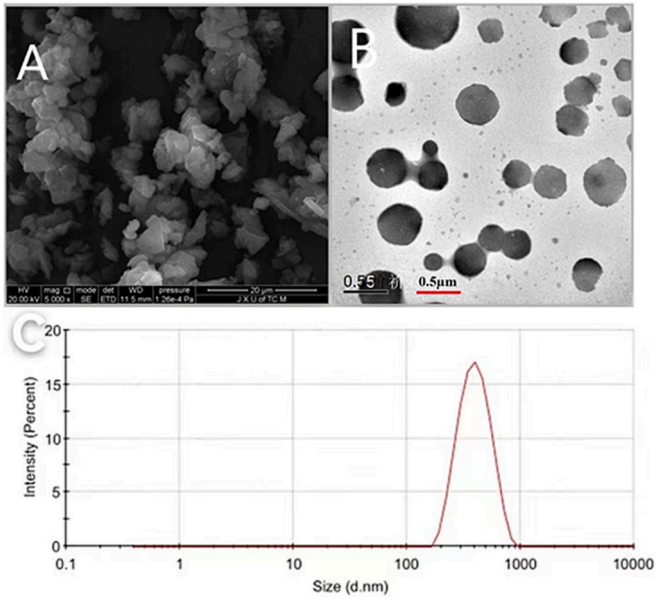

Fig. 2. SEM of Crude-SM (A), TEM of SM-NC (B) and the particle size distribution of silymarin nanocrystals (C).

3.3.2. The solubility study

As shown in Fig. 4 (B), the saturated solubility of both the silymarin crude drug and stabilizer-free silymarin nanocrystals was (98.04 ± 1.32) μg/mL and (138.07 ± 2.14) μg/mL, respectively. The results showed that the solubility of silymarin was increased by 1.41 times after being converted into drug nanocrystals ($P < 0.05$). The enhanced dissolution of silymarin with drug nanocrystals can be explained by the Noyes-Whitney equation (Wei et al., 2015b).

3.3.3. Stability study

As shown in Fig. 4 (C), The stabilizer-free silymarin nanocrystals, initially at a concentration of 2.0 mg/mL, exhibited an average particle size of 449.4 nm and a PDI of 0.281. Subsequent analysis revealed that storing the nanocrystals in the dark at room temperature for four days resulted in a slight increase in average particle size to 453.2 nm and PDI to 0.283, indicating stable behavior over the duration. Introduction of conventional space stabilizers (PVPK30, Tween 80, P188) and an electrostatic stabilizer (SDS) did not alter the particle size or PDI of the stabilizer-free silymarin nanocrystals after 0 and 4 days, confirming their stability. Overall, the stabilizer-free silymarin nanocrystals prepared at a low concentration of 2.0 mg/mL exhibited good stability for 4 days. Moreover, the addition of stabilizers to these nanocrystals also maintained their stability for the same duration, highlighting that the stability of our prepared stabilizer-free silymarin nanocrystals is comparable to, or even greater than, that of nanocrystals with added stabilizers.

3.3.4. Analysis of physical and chemical properties

When analyzing the physical and chemical properties of optimized drug nanocrystals, it was noted that the crystalline structure of the drug remained largely unchanged after nanocrystal formation, with only a slight decrease in crystallinity observed. This contrasts with previous studies where drug nanocrystal preparation often led to the formation of amorphous drug forms. This difference may be attributed to certain stabilizers potentially impeding crystal growth, resulting in the transformation of drug crystals into an amorphous state during nanocrystal preparation. To further investigate the stability of the prepared nanocrystals, our experimentation focused on spatial stability and electrostatic stability as the main mechanisms (Zhou et al., 2017). Various drug nanocrystals were synthesized using different space stabilizers (PVP K30, Tween 80, P 188) and electrostatic stabilizers (SDS). The stability of these drug nanocrystals, along with those containing various stabilizers, was evaluated over a four-day period at room temperature. The data showed that both the drug nanocrystals and those with stabilizers maintained consistent appearances throughout the study, showing no significant alterations. Additionally, particle size analysis indicated that the particle size of all drug nanocrystals remained virtually unchanged after 4 days of storage, indicating high stability. The stability of the drug nanocrystals prepared without stabilizers was found to be comparable to those containing stabilizers, both exhibiting high stability. Overall, the prepared drug nanocrystals demonstrated excellent stability performance as anticipated, with a focus on the apparent solubility and dissolution rate. The study revealed that drug nanocrystals can improve the saturation solubility of silymarin and enhance its dissolution rate in various aqueous media. In summary, the stabilizer-free silymarin nanocrystals formulated in this study showed favorable stability, along with significantly enhanced solubility and dissolution rates, laying the foundation for further investigation into oral absorption.

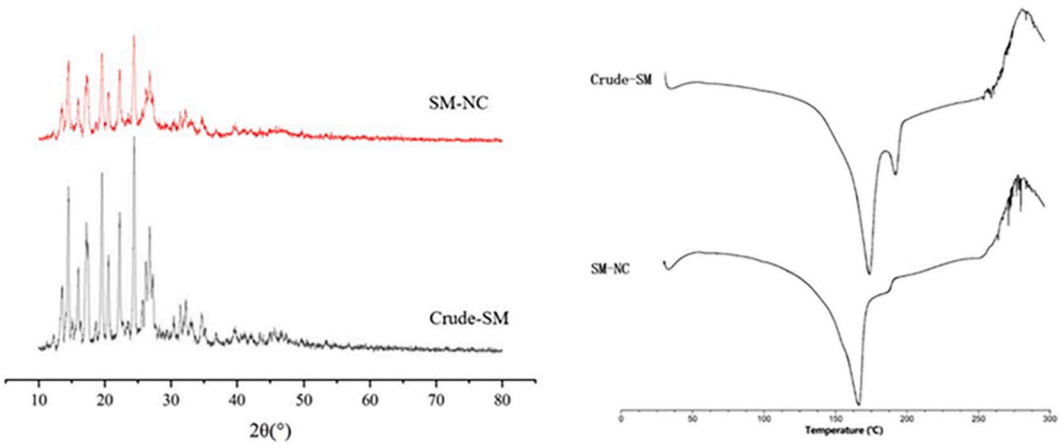

Fig. 3. XRD (left) and DSC (right) patterns of Crude-SM and SM-NC.

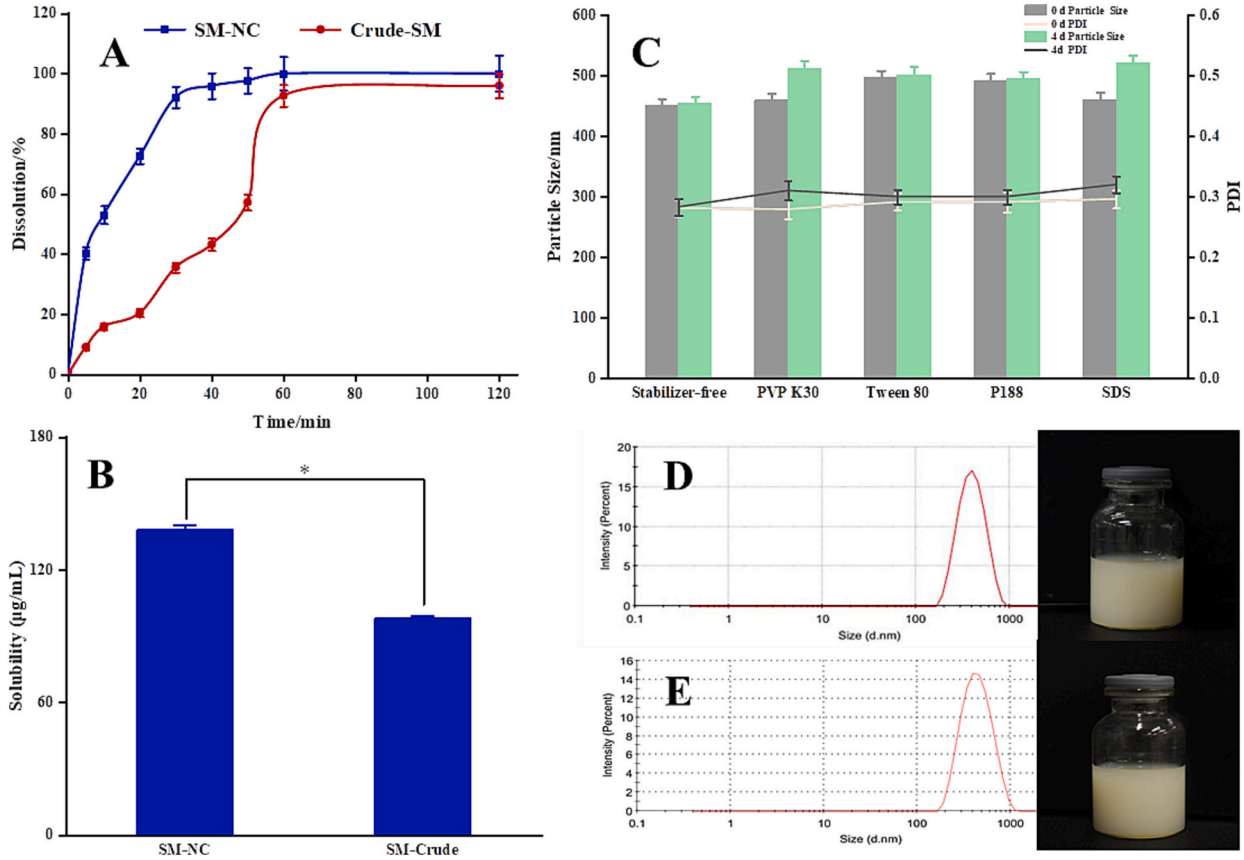

Fig. 4. The dissolution rate of Crude drug and nanocrystals in pure water at 37 °C (A), the solubility of raw drug and drug nanocrystals (B), the stability of silymarin nanocrystals modified by drugs and stabilizers (C) (mean ± SD, n = 3), the particle size distribution plots from day 1 and pictures of actual vials (D), the particle size distribution plots on day 4 and pictures of actual vials (E).

3.4. Study on the absorption-promoting mechanism

3.4.1. Cellular uptake

As shown in Fig. 5 (A), we conducted an analysis on the uptake of undissolved SM-NC, undissolved Crude-SM and dissolved Crude-SM by MDCK cells. Our findings indicate that the uptake of undissolved SM-NC increased with the rise of concentration, from 10.13 ± 0.41 μg/mg to 172.97 ± 8.40 μg/mg, within the concentration range of 31.3 μM to 500 μM. The uptake of undissolved Crude-SM also saw an increase in concentration from 4.97 ± 0.22 μg/mg to 64.26 ± 7.45 μg/mg, between the concentration range of 31.3 μM to 250 μM. When the concentration was 500 μM, there was no significant increase in uptake. This suggests that at a concentration of 250 μM, the cell uptake reached a peak of 79.54 μg/mg. In the high concentration range (250–500 μM), the uptake of undissolved SM-NC was significantly higher than that of Crude-SM ($P < 0.05$). Apparently, the main factor affecting absorption is that silymarin grains become smaller and more readily absorbed by the cells. It is evident from the figure that the intake of dissolved Crude-SM is low, ranging from 0.59 ± 0.12 μg/mg to 13.86 μg/mg.

As shown in Fig. 5 (B), stabilizer-free silymarin nanocrystals exhibited decreased uptake by MDCK cells at lower temperatures (4 °C) compared to controls samples. This suggests that stabilizer-free

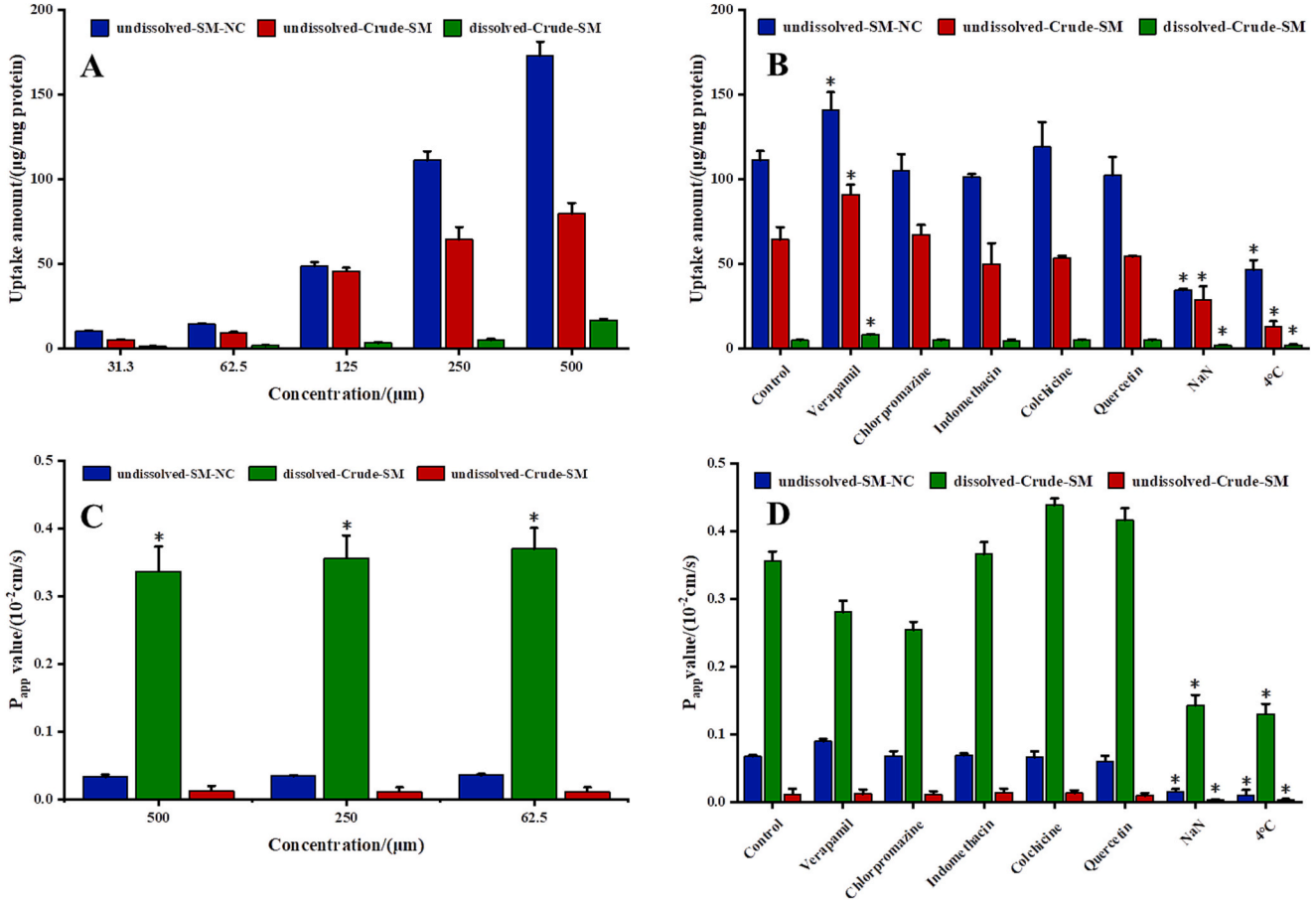

Fig. 5. The cellular uptake and monolayer transport of undissolved-SM-NC, undissolved-Crude-SM and dissolved-Crude-SM (mean ± SD, n = 3).

silymarin nanocrystals necessitate energy input for cellular penetration. The absorption of stabilizer-free silymarin nanocrystals was notably increased in the presence of verapamil (a P-gp protein inhibitor) and decreased in the presence of sodium azide (an energy inhibitor). This confirms that the drug requires energy to enter cells. No significant changes in drug uptake by MDCK cells were observed with treatment using chlorpromazine (a clathrin inhibitor), indomethacin (a caveolin inhibitor), colchicine (a macropinocytosis inhibitor), and quercetin (a non-clathrin inhibitor). To summarize, the entry mechanism of silymarin is influenced by the P-gp protein and is an energy-dependent process.

3.4.2. *Trans-membrane transport*

As shown in Fig. 5 (C), varying concentrations of undissolved SM-NC, dissolved Crude-SM, and undissolved Crude-SM were investigated to assess the transcellular transport capability of drug nanocrystals. The quantity of silymarin transported from the AP side to the BL side was quantified using the MDCK cell model. The findings revealed that as the concentrations of undissolved SM-NC, dissolved Crude-SM, and undissolved Crude-SM increased, the transport of undissolved SM-NC ranged from 0.032 * 10^{-2} cm/s to 0.035 * 10^{-2} cm/s, dissolved Crude-SM transport ranged from 0.34 * 10^{-2} cm/s to 0.37 * 10^{-2} cm/s, and undissolved Crude-SM transport was approximately 0.011 * 10^{-2} cm/s. Notably, the transport of insoluble SM-NC and Crude-SM was significantly lower compared to soluble Crude-SM ($P < 0.05$). Therefore, the principal transmembrane transport pathway (or oral absorption pathway) for solubilized drug molecules is through the cellular bypass route. In contrast, undissolved drug particles, including drug nanocrystals, despite being readily taken up by cells, exhibit lower transmembrane transport efficiency, likely due to inadequate intracellular transport mechanisms. This limitation may stem from the absence of an intracellular transporter pathway for nanocrystals to traverse from the AP side to the BL side within the cell. Therefore, enhancing the intracellular transport of nanocrystals, potentially through modifications with materials or other carriers, is crucial for improving their ability to facilitate oral drug uptake. Furthermore, it is evident that the cellular bypass pathway is not the primary transmembrane transport route for undissolved drug particles, including drug nanocrystals.

As shown in Fig. 5 (D), when the concentration was 250 μM, the undissolved SM-NC decreased from 0.035 * 10^{-2} cm/s to 0.010 * 10^{-2} cm/s at a temperature of 4 °C. Moreover, the transported quantity of dissolved Crude-SM also notably decreased from 0.36 * 10^{-2} cm/s to 0.13 * 10^{-2} cm/s. Various inhibitors like Verapamil, chlorpromazine, indomethacin, colchicine, and quercetin had minimal effects on undissolved SM-NC, dissolved Crude-SM and undissolved Crude-SM, but the transport rate significantly dropped with exposure to sodium azide, an energy inhibitor. Undissolved SM-NC decreased significantly from 0.035 ± 0.002 * 10^{-2} cm/s to 0.015 ± 0.004 * 10^{-2} cm/s ($p < 0.05$), while the transport quantity of dissolved Crude-SM decreased from 0.36 ± 0.04 * 10^{-2} cm/s to 0.14 ± 0.06 * 10^{-2} cm/s ($p < 0.05$). Undissolved Crude-SM translocation decreased from 0.011*10^{-2} to 0.003*10^{-2} at 4 °C and sodium azide. The results suggest that temperature and energy play crucial roles in cell transmembrane transport. The study investigated the transportation of undissolved SM-NC and dissolved Crude-SM under various conditions, revealing that undissolved SM-NC transportation was lower than that of dissolved Crude-SM, consistent with findings at different concentrations.

3.4.3. *Analysis of absorption mechanism*

Epithelial cells in multicellular organisms act as a barrier separating

internal and external environments. Substances can move through these cells via two pathways: transcellular and paracellular. The permeability of the paracellular pathway is regulated by tight junctions (TJs) located at the apical region of the cell complex (Farquhar and Palade, 1963; Staehelin, 1973; Powell, 1981). Changes in life activities, like water intake, can alter the osmotic pressure of the external environment. MDCK cells, known for their 'leaky' properties, have been extensively studied regarding paracellular transport characteristics. Research shows that the osmotic gradient plays a significant role in regulating paracellular transport in MDCK cells (Tokuda et al., 2016). It is important to note that different cell types respond uniquely to the osmotic gradient and paracellular transport.

In this study, MDCK cells were utilized as a cellular model to investigate the impact of stabilizer-free silymarin nanocrystals on enhancing silymarin cellular uptake and transport. The results indicated that the uptake of undissolved SM-NC, undissolved Crude-SM, and dissolved Crude-SM by MDCK cells increased with rising concentrations within the 31.3–500 μM range. Undissolved SM-NC exhibited higher uptake than undissolved Crude-SM, while undissolved Crude-SM showed greater uptake than dissolved Crude-SM. Verapamil, a protein inhibitor, notably enhanced the uptake of undissolved SM-NC, undissolved Crude-SM, and dissolved Crude-SM, whereas low temperature and the energy inhibitor sodium azide led to a significant decrease in uptake of undissolved SM-NC, undissolved Crude-SM and dissolved Crude-SM. The transmembrane transport results indicated that undissolved SM-NC and undissolved Crude-SM exhibited significantly lower transport rates compared to dissolved Crude-SM when low temperature and energy inhibitors were applied. The cellular bypass pathway has been identified as the primary transmembrane transport route for dissolved drug molecules. In contrast, for undissolved drug particles (undissolved SM-NC and undissolved Crude-SM), cellular uptake was found to be higher, although intracellular transport efficiency may be suboptimal. This study emphasizes a significant finding: Some researchers argue that nanocrystals can enhance drug transmembrane transport via an endocytosis-mediated pathway (Fu et al., 2013; Zhu et al., 2021), the reality is that nanocrystals are indeed heavily endocytosed by cells. However, the lack of intracellular ability to move nanocrystals from the apical (AP) to the basolateral (BL) side of the cell results in poor translocation efficiency. Therefore, we believe that the ability of nanocrystals to promote their oral drug uptake can be improved and achieved by modifying the drug or using carriers to increase the efficiency of intracellular transport.

3.5. Pharmacokinetic study in vivo

Fig. 6 (A) illustrates the drug-time curve area after the oral administration of silymarin in rats, showing significant double peaks in maximum concentration for both silymarin crude drugs and stabilizer-free silymarin nanocrystals, indicating hepato-enteral circulation properties. Fig. 6 (B) presents the silymarin concentration-time curve following a tail vein injection in rats, with pharmacokinetic parameters detailed in Table 1. Compared to the crude drugs, the stabilizer-free silymarin nanocrystals resulted in a larger area under the plasma concentration-time curve, and stabilizer-free silymarin nanocrystals exhibited a higher peak plasma level (2.27 times, $P < 0.05$). This suggests that the absorption of stabilizer-free silymarin nanocrystals is faster and more effective due to a quicker time to reach peak plasma concentration and a higher concentration level. In conclusion, the improved oral bioavailability of silymarin in rats can be attributed to the reduction in particle size and increased dissolution achieved by preparing the drug into nanocrystals. These findings highlight the potential of drug nanocrystals for enhancing drug delivery, as their design promotes rapid absorption in the early stages, leading to complete and improved absorption.

The solubility of stabilizer-free silymarin nanocrystals, prepared without stabilizers in this study, was found to be 1.41 times higher compared to the crude drugs. When tested in pure water, the stabilizer-free silymarin nanocrystals exhibited a dissolution rate of around 92.2 % within 30 min, while the crude drugs only achieved a rate of 38.5 %. This indicates a significant enhancement in the dissolution rate of silymarin with the use of drug nanocrystals. Additionally, it was noted that the solubility of the drug nanocrystals surpassed that of the crude drugs in pure water. Previous studies have shown the impact of particle size on dissolution rate and solubility (Wang et al., 2010). Drug nanocrystals in the nanoscale range can navigate through small capillaries and avoid phagocyte-mediated clearance, thereby enhancing bioavailability.

Table 1
Pharmacokinetic parameters following single dose administration of SM-NC, crude SM, and SM injection. (n = 5).

Pharmacokinctic parameters	SM-NC,oral (50 mg/kg)	Crude-SM,oral (50 mg/kg)	SM solution,iv (4 mg/kg)
$AUC_{(0-t)}$/μg·L^{-1}	6114.94 ± 344.46*	5073.84 ± 833.34	5564.01 ± 271.40
$AUC_{(0-\infty)}$ /μg·L^{-1}	8635.75 ± 792.29*	5823.24 ± 799.01	6466.34 ± 1159.13
C_{max}/μg·L^{-1}	1585.70 ± 213.98*	698.46 ± 152.92	15,529.12 ± 5763.62
$t_{1/2}$/h	18.79 ± 7.02	8.76 ± 1.41	9.45 ± 4.44
CLz/F	5.83 ± 0.51	8.72 ± 1.32	0.64 ± 0.14
T_{max}/h	1.00 ± 0.00	1.19 ± 0.55	0.02 ± 0.00
Fa/%	10.68	7.20	100.00
Fr/%	148.29	100.00	/

Note: Each value represents mean ± SD. (n = 5) *P < 0.05 compared to crude SM.

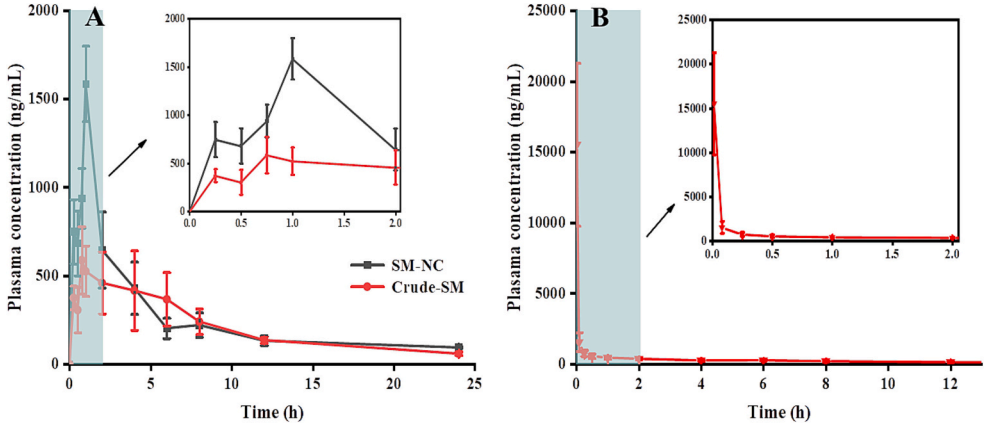

Fig. 6. Drug-time curve after oral administration of SM-NC and Crude-SM in rats (A) and Drug-time curve after intravenous injection of silymarin in rats (B) ($n = 5$).

4. Conclusions

In this study, stabilizer-free silymarin nanocrystals were formulated and evaluated. The saturated solubility and dissolution rate of stabilizer-free silymarin nanocrystals in pure water were increased compared to the crude drug. However, in terms of oral uptake and transcellular transport, we found that the stabilizer-free silymarin nanocrystals showed a significant increase in uptake but poorer transmembrane transport performance. The results of pharmacokinetic parameters indicated that SM-NC improved oral bioavailability in rats compared to Crude-SM. Therefore, if there is a need to improve the ability of nanocrystals to promote oral drug uptake, the intracellular transport of nanocrystals must be improved (with modifications or other carriers for this purpose).

CRediT authorship contribution statement

Liangxing Tu: Writing – original draft. **Ping Han:** Conceptualization. **Yongbing Sun:** Conceptualization. **Yi Jin:** Conceptualization. **Kaili Hu:** Conceptualization. **Meng Cheng:** Writing – review & editing. **Yisen Shao:** Writing – review & editing. **Jianfang Feng:** Writing – review & editing. **Fangying Yuan:** Methodology, Investigation.

Declaration of competing interest

The authors declare that they have no known competing financial interests or personal relationships that could have appeared to influence the work reported in this paper.

Data availability

Data will be made available on request.

Acknowledgements

This research was funded by the National Natural Science Foundation of China (81960717, 82304730), the Project of Academic and Technical Leaders in Major Disciplines in Jiangxi Province (20212BCJL23060), the Jiangxi University of Chinese Medicine Science and Technology Innovation Team Development Program (CXTD-22004, CXTD-22008) and the PhD Startup Foundation of Affiliated Hospital of Jiangxi University of Chinese Medicine (23KYQDZJ02).

References

Abrol, S., Trehan, A., Katare, O.P., 2005. Comparative study of different silymarin formulations:formulation, characterisation and *in vitro/in vivo* evaluation. Curr. Drug Deliv. 2 (1), 45–51.

Arcari, M., Brambilla, A., Brandt, A., Caponi, R., Corsi, G., Rella, M.D., Solinas, F., Wachter, W.P., 1992. A new inclusion complex of silibinin and beta-cyclodextrins: *in vitro* dissolution kinetics and *in vivo* absorption in comparison with traditional formulations. Boll. Chim. Farm. 131 (5), 205–209.

Bahmani, M., Shirzad, H., Rafieian, S., Rafieian-Kopaei, M., 2015. *Silybum marianum*: beyond Hepatoprotection[J]. J. Evid. Based Complement. Altern. Med. 20 (4), 292–301.

Burczynski, F.J., Wang, G.Q., Nguyen, D., Chen, Y.F., Smith, H.J., Gong, Y.W., 2012. Silymarin and hepatoprotection. Zhong Nan Da Xue Xue Bao Yi Xue Ban 37 (1), 6–10.

Choi, J.Y., Yoo, J.Y., Kwak, H.S., Nam, B.U., 2005. Role of polymeric stabilizers for drug nanocrystal dispersions. Curr. Appl. Phys. 5 (5), 472–474.

Ding, T., Tian, S., Zhang, Z., Gu, D., Chen, Y., Shi, Y., Sun, Z., 2001. Determination of active component in silymarin by RP-LC and LC/MS. J. Pharm. Biomed. Anal. 26 (1), 155–161.

El-Nahas, A.E., Allam, A.N., El-Kamel, A.H., 2017. Mucoadhesive buccal tablets containing silymarin Eudragit-loaded nanoparticles: formulation, characterisation and ex vivo permeation. J. Microencapsul. 34 (5), 463–474.

Farquhar, M.G., Palade, G.E., 1963. Junctional complexes in various epithelia. J. Cell Biol. 17, 375–412.

Federico, A., Dallio, M., Fabio, G.D., Zarrelli, A., 2015. Silybin-phosphatidylcholine complex protects human gastric and liver cells from oxidative stress. In Vivo 29 (5), 569–575.

Fu, Q., Sun, J., Ai, X., Zhang, P., Li, M., Wang, Y., Liu, X., Sun, Y., Sui, X., Sun, L., Han, X., Zhu, M., Zhang, Y., Wang, S., He, Z., 2013. Nimodipine nanocrystals for oral bioavailability improvement: role of mesenteric lymph transport in the oral absorption. Int. J. Pharmaceut. 448 (1), 290–297.

Ghosh, A., Biswas, S., Ghosh, T., 2011. Preparation and evaluation of silymarin beta-cyclodextri molecular inclusion complexes. J. Young Pharm. 3 (3), 205–210.

Goke, K., Lorenz, T., Repanas, A., Schneider, F., Steiner, D., Baumann, K., Bunjes, H., Dietzel, A., Finke, J.H., Glasmacher, B., 2018. Novel strategies for the formulation and processing of poorly water-soluble drugs. Eur. J. Pharm. Biopharm. 126, 40–56.

Hwang, D.H., Kim, Y.I., Cho, K.H., Poudel, B.K., Choi, J.Y., Kim, D.W., Shin, Y.J., Bae, O. N., Yousaf, A.M., Yong, C.S., Kim, J.O., Choi, H.G., 2014. A novel solid dispersion system for natural product-loaded medicine: silymarin-loaded solid dispersion with enhanced oral bioavailability and hepatoprotective activity. J. Microencapsul. 31 (7), 619–626.

Kadam, R., Ghawali, J., Waespy, M., Maas, M., Rezwan, K., 2020. Janus nanoparticles designed for extended cell surface attachment. Nanoscale 12 (36), 18938–18949.

Kesisoglou, F., Panmai, S., Wu, Y., 2007. Nanosizing—oral formulation development and biopharmaceutical evaluation. Adv. Drug Deliv. Rev. 59, 631–644.

Kirtane, A.R., Kalscheuer, M.S., Panyam, J., 2013. Exploiting nanotechnology to overcome tumor drug resistance: challenges and opportunities. Adv. Drug Deliv. Rev. 65 (13–14), 1731–1747.

Kvasnicka, F., Biba, B., Sevcik, R., Voldrich, M., Kratka, J., 2003. Analysis of the active components of silymarin. J. Chromatogr. A 990 (1–2), 239–245.

Lee, J., Le, S.J., Choi, J.Y., Yoo, J.J., Ahn, C.H., 2005. Amphiphilic amino acid copolymers as stabilizers for the preparation of nanocrystal dispersion. Eur. J. Pharm. Sci. 24 (5), 441–449.

Li, F.Q., Hu, J.H., 2004. Improvement of the dissolution rate of silymarin by means of solid dispersions. Chem. Pharm. Bull. (Tokyo). 52 (8), 972–973.

Liu, Y., Xue, Z.F., Hou, X.F., Xie, X.M., Shi, J.P., Shen, J.Y., He, Y.Z., Wang, Z., Feng, N.P., 2019. Functional lipid polymeric nanoparticles for oral drug delivery: rapid mucus penetration and improved cell entry and cellular transport. Nanomed-Nanotechnol. 21, 102075.

Liu, J.L., Sun, Y.B., Cheng, M., Liu, Q.M., Liu, W., Gao, C., Feng, J.F., Jin, Y., Tu, L.X., 2021. Improving oral bioavailability of luteolin nanocrystals by surface modification of sodium dodecyl sulfate. AAPS PharmSciTech 22 (3), 133.

Lu, C., Lu, Y., Chen, J., Zhang, W.T., Wu, W., 2007. Synchronized and sustaine release of multiple components in silymarin from erodible glyceryl monostearate matrix system. Eur. J. Pharm. Biopharm. 66 (2), 210–219.

Lu, Y., Li, Y., Wu, W., 2016. Injected nanocrystals for targeted drug delivery. Acta Pharm. Sin. B 6, 106–113.

Maisel, K., Ensign, L., Reddy, M., Cone, R., Hanes, J., 2015. Effect of surface chemistry on nanoparticle interaction with gastrointestinal mucus and distribution in the gastrointestinal tract following oral and rectal administration in the mouse. J. Control. Release 197, 48–57.

Morazzoni, P., Magistretti, M.J., Giachetti, C., Zanolo, G., 1992. Comparative bioavailability of Silipide, a new flavanolignan complex, in rats. Eur. J. Drug Metab. Pharmacokinet. 17 (1), 39–44.

Palle, S., Neerati, P., 2017. Enhancement of oral bioavailability of rivastigmine with quercetin nanoparticles by inhibiting CYP3A4 and esterases. Pharmacol. Rep. 69 (2), 365–370.

Ponchel, G., Montisci, M.J., Dembri, A., Durrer, C., Duchêne, D., 1997. Mucoadhesion of colloidal particulate systems in the gastro-intestinal tract. Eur. J. Pharm. Biopharm. 44, 25–31.

Popov, A., Enlow, E., Bourassa, J., Chen, H.M., 2016. Mucus-penetrating nanoparticles made with "mucoadhesive" poly(vinyl alcohol). Nanomedicine 12 (7), 1863–1871.

Powell, D.W., 1981. Barrier function of epithelia. Am. J. Phys. 241 (4), G275–G288.

Raj, P.V., Kumar, N., Prateek, J., Sankhe, M.N., 2010. Effect of Lecithin and silymarin on D-galactosamine induced toxicity in isolated hepatocytes and rats. Indian J. Clin. Biochem. 25 (2), 169–174.

Shangguan, M.Z., Lu, Y., Qi, J.P., Han, J., Tian, Z.Q., Xie, Y.C., Hu, F.Q., Yuan, H.Y., Wu, W., 2014. Binary lipids-based nanostructured lipid carriers for improved oral bioavailability of silymarin. J. Biomater. Appl. 28 (6), 887–896.

Staehelin, L.A., 1973. Further observations on the fine structure of freeze-cleaved tight junctions. J. Cell Sci. 13 (3), 763–786.

Tokuda, S., Hirai, T., Furuse, M., 2016. Effects of Osmolality on Paracellular Transport in MDCK II Cells. PLoS One 11 (11), e166904.

Tu, L.X., Cheng, M., Sun, Y.B., Fang, Y., Liu, J.L., Liu, W., Feng, J.F., Jin, Y., 2020a. Fabrication of ultra-small nanocrystals by formation of hydrogen bonds: *in vitro* and *in vivo* evaluation. Int. J. Pharmaceut. 573, 118730.

Tu, L.X., Cheng, M., Sun, Y.B., Fang, Y.Y., Liu, J.L., Liu, W., Feng, J.F., Jin, Y., 2020b. Fabrication of ultra-small nanocrystals by formation of hydrogen bonds: *in vitro* and *in vivo* evaluation. Int. J. Pharmaceut. 573, 118730.

Viswanadh, M.K., Vikas, Jha A., Reddy Adena, S.K., Mehata, A.K., Priya, V., Neogi, K., Poddar, S., Mahto, A.K., Muthu, M.S., 2020. Formulation and *in vivo* efficacy study of cetuximab decorated targeted bioadhesive nanomedicine for non-small-cell lung cancer therapy. Nanomedicine (London) 15 (24), 2345–2367.

Wang, Y.C., Zhang, D., Liu, Z.P., Liu, G.P., Duan, C.X., Jia, L.J., Feng, F.F., Zhang, X.Y., Shi, Y.Q., Zhang, Q., 2010. *In vitro* and *in vivo* evaluation of silybin nanosuspensions for oral and intravenous delivery. Nanotechnology 21 (15), 155104.

Wang, X.Y., Chen, Y.H., Dahmani, F.Z., Yin, L.F., Zhou, J.P., Yao, J., 2014. Amphiphilic carboxymethyl chitosan-quercetin conjugate with P-gp inhibitory properties for oral delivery of paclitaxel. Biomaterials 35, 7654–7665.

Wei, L.S., Ji, Y.X., Gong, W., Kang, Z.Q., 2015a. Preparation, physical characterization and pharmacokinetic study of paclitaxel nanocrystals. Drug Dev. Ind. Pharm. 41 (8), 1343–1352.

Wei, L.S., Ji, Y.X., Gong, W., Kang, Z.Q., Meng, M., Zheng, A., Zhang, X.Y., Sun, J.X., 2015b. Preparation, physical characterization and pharmacokinetic study of paclitaxel nanocrystals. Drug Dev. Ind. Pharm. 41 (8), 1343–1352.
Xu, P.F., Yin, Q., Shen, J.N., Chen, L.L., 2013. Synergistic inhibition of breast cancer metastasis by silibinin-loaded lipid nanoparticles containing TPGS. Int. J. Pharmaceut. 454 (1), 21–30.
Yang, K.Y., Hwang, D.H., Yousaf, A.M., Dong, W.K., Shin, Y.J., Bae, O.N., Kim, Y.I., Kim, J.O., Yong, C.S., Choi, H.G., 2013. Silymarin-loaded solid nanoparticles provide excellent hepatic protection: physicochemical characterization and *in vivo* evaluation. Int. J. Nanomedicine 8, 3333–3343.
Yi, Y.N., Tu, L.X., Hu, K.L., Wu, W., Feng, J.F., 2015. The construction of puerarin nanocrystals and its pharmacokinetic and *in vivo–in vitro* correlation (IVIVC) studies on beagle dog. Coll. Surf. B 133, 164–170.
Zhang, E.H., Xing, R.G., Liu, S., Qin, Y.K., Li, K.C., Li, P.C., 2019. Advances in chitosan-based nanoparticles for oncotherapy. Carbohydr. Polym. 222, 115004.
Zhou, Y.Q., Du, J., Wang, L.L., Wang, Y.C., 2017. Nanocrystals technology for improving bioavailability of poorly soluble drugs: a mini-review. J. Nanosci. Nanotechnol. 17 (1), 18–28.
Zhu, H., Brinda, B.J., Chavin, K.D., Bernstein, H.J., Patrick, K.S., Markowitz, J.S., 2013. An Assessment of Pharmacokinetics and Antioxidant Activity of Free Silymarin Flavonolignans in Healthy Volunteers. A Dose Escalation Study, pp. 1679–1685.
Zhu, Y.J., Fu, Y., Zhang, A., Wang, X.L., Zhao, Z.Q., Zhang, Y., Ying, T., Gou, J.X., Wang, Y.J., He, H.B., Tang, X., 2021. Rod-shaped nintedanib nanocrystals improved oral bioavailability through multiple intestinal absorption pathways. Eur. J. Pharm. Sci. 168, 106047.